Investigating Fuel-Cell Transport Limitations using Hydrogen Limiting Current

Franz B. Spingler, Adam Phillips, Tobias Schuler, Michael C. Tucker, Adam Z. Weber

Energy Conversion Group, Energy Technologies Area, Lawrence Berkeley National Laboratory, 1 Cyclotron Road, Berkeley CA 94720, USA

Reducing mass-transport losses in polymer-electrolyte fuel cells (PEFCs) is essential to increase their power density and reduce overall stack cost. At the same time, cost also motivates the reduction in expensive precious-metal catalysts, which results in higher local transport losses in the catalyst layers. In this paper, we use a hydrogen-pump limiting-current setup to explore the gas-phase transport losses through PEFC catalyst layers and various gas-diffusion and microporous layers. It is shown that the effective diffusivity in the gas-diffusion layers is a strong function of liquid saturation. In addition, it is shown how the catalyst layer unexpectedly contributes significantly to the overall measured transport resistance. This is especially true at low catalyst loadings. It is also shown how the various losses can be separated into different mechanisms including diffusional processes and mass-dependent and independent ones, where the data suggests that a large part of the transport resistance in CLs cannot be attributed to a gas-phase diffusional process. The technique is promising for deconvoluting transport losses in PEFCs.

Introduction

Performance limitations of polymer-electrolyte fuel cells (PEFCs) can generally be attributed to several causes: mixed potentials due to reactant gas crossover, finite reaction kinetics, ohmic resistances throughout the cell, and concentration losses due to limited mass transport to the reaction sites [1]. These latter losses are increasingly important as one tries to increase overall power density of a cell in order to decrease the cell number in a stack and thus overall cost. Figure 1 shows a schematic of the oxygen pathway from the flow field to the reaction site: gas-phase diffusion governs the transport through the diffusion media (DM), composed of a gas-diffusion layer (GDL) and perhaps microporous layer (MPL), and the bulk of the catalyst layer (CL). Subsequently, oxygen needs to penetrate through the ionomer film covering the Pt sites. As detailed in Figure 1, there is likely to be a gas/ionomer film interface, an ionomer film resistance, and an ionomer/Pt interface slowing down oxygen transport [2, 3]. These resistances are compounded for lower-cost low-loaded CLs (< 0.1 mg_{Pt}/cm^2) due to the increased local flux through them to the reaction site, which has been observed experimentally [4-7] and limits the Pt loading decreases.

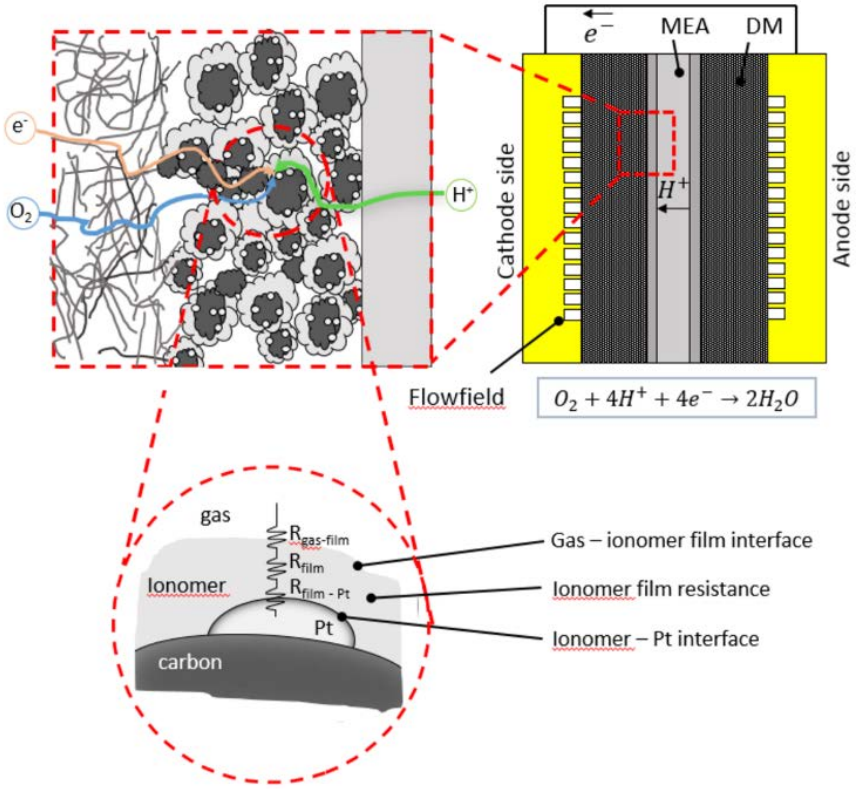

Figure 1: Schematic of oxygen diffusion losses in a fuel-cell cathode

A typical way to measure the various transport-related losses involves the measurement of a dilute-oxygen limiting current in an operating cell. However, this requires the understanding and deconvolution of various transport losses in DM and CLs. The possible existence of oxide formation and complicated oxygen-reduction-reaction kinetics and the production of water and heat further complicate the analysis. In addition, this technique does not allow the assessment of properties such as effective diffusivity as a function of liquid saturation as one cannot readily control the latter. To overcome the above issues, researchers have opened up the parameter space by stacking DM [8], diluting the reactant gases in different carrier gases [4, 8], and varying the cell pressure [9-11]. Researchers have also used various ex-situ techniques to characterize DM. These include Loschmidt diffusion cells, which allow for the observation of non-stationary diffusion between two gas chambers separated by a DM [12-

14] and diffusion bridges, which allow for a stationary measurement of the pressure drop through a DM [15-19]. Another ex-situ method for diffusivity analysis is electrochemical diffusimetry, where the DM is soaked with an electrolyte and the effective ionic conductivity is used to obtain the effective diffusivity via analogy between Fick's and Ohm's law. This method has been used to derive in- and through-plane diffusivity at different compressions and PTFE loadings [20, 21]. Also, x-ray computed tomography has been used to examine tortuosity [22] and effective diffusivity at various saturations [23]. These values have been obtained as well in an easier and more controlled setup using a hydrogen-limiting current in a hydrogen-pump mode [24]; however, that study required an effective channel hydrogen concentration that was lower than expected in order to describe the data.

Similar to measuring the resistance in the DM, there is strong interest in measuring the resistances in the CL as well. As noted above, this is typically accomplished using an *in-situ* limiting current experiment. Mashio et al. [25] reported an increase in the overall CL resistance with increasing ionomer loadings, which they attributed to a change in bulk porosity with ionomer content inside the CL. Sakai et al. [5] continue the aforementioned experiments with different CL platinum loadings and suggested a local resistance at the platinum particle surface, which became more prominent as the platinum loading was reduced. Nonoyama et al. [4] found that permeation through the ionomer film covering the platinum sites was a major contribution to the overall oxygen transport resistance in the CL. Studying a wide range of platinum loadings, Greszler et al. [6] concluded that interfacial transport or a slow adsorption step in the oxygen pathway may be responsible for the high resistance related to the ionomer film. Using the same experimental procedure, Owejan et al. [26] further varied the Pt/C ratio and, and using a single-particle model, found that taking

into account interfacial resistances at both the gas/ionomer and ionomer/platinum interfaces yielded the best fit to the experimental data. Iden et al. [27] proposed an alternative *in-situ* method based on gas crossover through the membrane to study hydrogen vs. oxygen transport resistances near the platinum surface. Also, ex-situ approaches using Nafion thin films cast on platinum electrodes have been demonstrated [28, 29]. Finally, in one of the earlier studies, Yoon and Weber [30] modeled the extra resistance and demonstrated that due to isolated catalyst particles, the effective diffusion pathlength for the oxygen increased, which is somewhat similar to the analysis of Debe [31] who examined it from a probability perspective.

In this paper, we propose an integrated approach for the study of DM and CL transport resistance by establishing a transport-limited hydrogen-oxidation reaction (i.e., hydrogen-pump mode), which alleviates the water and heat generation and oxygen influences discussed above. We build upon the work of Hwang and Weber by exploring the mechanisms in more detail and applying them to microporous layers (MPLs) and CLs.

Experimental

Small-scale cell.

A small-scale experimental cell of 1 cm^2 maximum active area was used, as described in Hwang and Weber [24] and shown in Figure 2. Gold-plated straight flow fields with 5 channels of 0.4 mm width and 0.2 mm wide ribs were used. To control the working electrode active area, a thin conductive copper foil (0.04 mm) with an aperture hole of 1/4 inch diameter was placed between the flow field and the working electrode DM. The resulting active area is 0.35 cm^2. Compression was controlled with PTFE and PVC gaskets that

matched the respective sample thickness exactly or were thinner by a maximum of 5% (i.e., 5% GDL compression). The entire assembly is then compressed by about 200 lb/in^2 to ensure it is gas tight. The pressure was estimated with pressure-sensitive paper (Prescale, Fuji Film). Ohmic resistance measured with electrochemical impedance spectroscopy showed no major change in resistance when thinner gaskets were used to compress the samples to higher levels, indicating that the low compressions obtained with matching gaskets provided sufficient electrical contact between the different cell layers as discussed in supporting information.

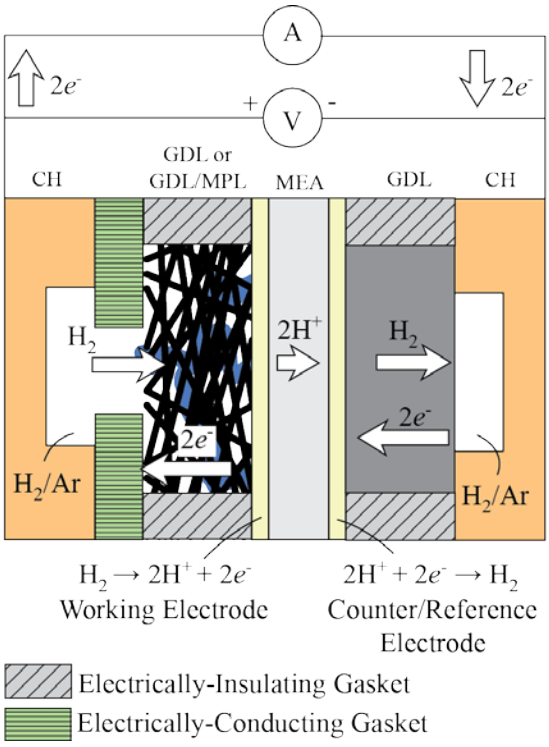

Figure 2: Schematic of experimental hydrogen-pump limiting-current cell.

Theory

The transport resistances of DM and CL were obtained from the transport limited HOR current in a hydrogen-pump cell. The advantage of the hydrogen reaction is that no water is produced at the working electrode, so the cell humidity can be precisely controlled via the relative humidity (RH) of the inlet gases. Furthermore, hydrogen kinetics on platinum are facile. The hydrogen supplied to the cell was highly diluted in argon, which slows down the diffusion, thus magnifying the transport resistances. The governing reactions for the hydrogen pump, as shown in Figure 2, are

$$H_2 \rightarrow 2H^+ + 2e^- \quad [1]$$

at the working electrode and

$$2H^+ + 2e^- \rightarrow H_2 \quad [2]$$

at the counter electrode. A potential (0.35 V) is used that results in a limiting current for the supplied hydrogen. This current can be related to the flux of hydrogen molecules to the working electrode,

$$N_{H_2} = \frac{i}{2F} \quad [3]$$

where N_{H2} is the flux of hydrogen, i is the electric current density and F is Faraday's constant. The driving force for the hydrogen flux is the hydrogen concentration gradient in the through-plane direction. To take the consumption of hydrogen along the flow field channels

into account, a mass flow balance for the flow field is used to obtain the average concentration of hydrogen in the flow field, $c_{H2,ff}$

$$c_{H_{2,ff}} = \frac{\dot{n}_{H_2,feed} - \frac{1}{2}\dot{n}_{H_2}}{\dot{n}_{H_2,feed}} c_{H_2,feed} \quad [4]$$

where $c_{H2,feed}$ and $n_{H2,feed}$ are the hydrogen concentration and hydrogen mass flow of the inlet gas, and n_{H2} is the mass consumption of hydrogen. In experiments using 1000 ppm hydrogen in argon, the average hydrogen concentration in the flow field changes only 3 to 9% (i.e., a stoichiometry of 10 to 20. Assuming that the hydrogen concentration at the reaction sites is zero (i.e. limiting current) and taking a resistance in series approach, one may write

$$R_{total} = \frac{c_{H_2,ff}}{N_{H_2}} = R_{foil} + R_{DM} + R_{CL} \quad [5]$$

where R_{total} is the total diffusional resistance in s/m, equaling the sum of the bulk diffusion resistance along the thickness of the copper foil, R_{foil}, the diffusion resistance through the diffusion medium, R_{DM}, and the average transport resistance from the surface of the CL to the reaction sites, R_{CL}. After substracting R_{foil}, which is equal to the binary diffusion coefficient of hydrogen in argon divided by the foil thickness (0.04 mm), R_{DM} and R_{CL} remain to be discriminated. The approach chosen in this study was to perform limiting current measurements with up to five DM stacked upon each other, and fitting R_{total} to

$$R_{total}(n) = R_{foil} + R_{CL} + n \cdot R_{DM} \quad [6]$$

where *n* is the number of DM. The diffusion medium resistances R_{DM} were converted into effective through-plane diffusivities $\langle D_{DM} \rangle$ using the measured DM thickness t_{DM} and a correction factor k_{tp} for the edge effect caused by in-plane diffusion,

$$\left\langle D_{DM} \right\rangle = t_{DM} / R_{DM} \cdot k_{tp} \qquad [7]$$

Division of $\langle D_{DM} \rangle$ by the binary diffusion coefficient of hydrogen in argon, $D_{H_2,Ar}$ results in a quantity that can be related to two functions representing the material properties of the DM,

$$\frac{\left\langle D \right\rangle}{D_{H_2,Ar}} = f(\varepsilon) \cdot g(S) \qquad [8]$$

where ε is the porosity of the DM, S is the liquid-water saturation, and *f* and *g* are empirical functions.

The in-plane diffusivity of a DM is known to be inherently larger than the through-plane diffusivity as a result of the horizontal alignment of fibers. Experimental data in the literature suggests ratios (in-plane:through-plane diffusivities), of 1 to 2.5 for bare DMs [21, 32] and notably, 66 for a MPL coated DM [15]. In the experimental cell used in this study, the DM sample has a larger diameter than the aperture in the copper foil. As a result, in-plane diffusion does not only allow the reactant gas to spread over the ribs of the flow field, but also helps through-plane transport by enlarging the diffusion cross-section. The impact of this effect on the measured diffusivity was estimated for 1 to 5 stacked DM by a simplistic 3D diffusion model solved with Comsol Multiphysics, resulting in the correction factor k_{tp} = 0.7 to 0.84, respectively.

As Figure 1 suggests, reactant transport in the CL could be broken down into diffusion through the bulk and a local resistance around the reaction sites. Considering typical pore-size distributions [4, 32] of a CL, transport through the bulk of the CL may be described by molecular diffusion (larger pores) and Knudsen diffusion (smaller pores). The molecular diffusion coefficient $D_{A,B}$ in cm²/s for a binary mixture of gases can be estimated with the Fuller-Schettler-Giddings equation,

$$D_{A,B} = \frac{0.001 \cdot T^{1.75}}{P(\nu_A^{1/3} + \nu_B^{1/3})^2} \sqrt{\frac{1}{M_A} + \frac{1}{M_B}} \qquad [9]$$

where T is the temperature in K, P is the pressure in atmospheres, and M_i and ν_i are the molecular weight and volume of species *i*, respectively. The Knudsen diffusion coefficient D_A^{Kn} in m²/s for a long and narrow pore is:

$$D_A^{Kn} = \frac{1}{3}\left(\frac{8RT}{\pi M_A}\right)^{1/2} d_p \qquad [10]$$

where R is the ideal-gas constant and d_p is the pore diameter. As can be seen from the equations above, molecular diffusion is inversely proportional to pressure while Knudsen diffusion is pressure independent. Gas pressure was varied from 1 to 3 atm in order to separate molecular and Knudsen contributions. Also, as seen above, both molecular and Knudsen diffusion coefficients depend on the molecular weight of the diffusing species. Changing the reacting gas from hydrogen to deuterium, whose molecular weight is twice as high, should lower the diffusion coefficient accordingly. In the case of molecular diffusion, the factor should be ca. $\sqrt{1.91}$, for Knudsen diffusion it should be ca. $\sqrt{2}$.

Experiment operation

Both electrodes were fed with 1000 ppm hydrogen (or deuterium) diluted in argon. The counter electrode was always fed with 2% hydrogen in argon. Gas flowrates at the working and counter electrode were 500 and 200 cm^3 min^{-1}, respectively. Flowrate, pressure, and RH were controlled with a fuel-cell test station (Fuel Cell Technologies Inc.), flow controllers (MKS Instruments), and bubblers. A fully humidified gas stream was obtained by humidification in two stages: the gases were first saturated at 5°C higher than the cell temperature in a bubbler inside the fuel-cell test station and then passed through a second, external bubbler at the cell operating temperature (20°C). This fully humidified gas stream could then be mixed with a dry gas stream at any ratio. RH was monitored by means of a Vaisala HMT337 RH-Meter. Throughout this study, RH was kept at 90%. Cell voltage was controlled with a Bio-Logic VMP3 potentiostat.

New MEAs were conditioned by 20 cyclic-voltammetry cycles from 0.05 V to 1.2 V at 50 mV/s and subsequent potential hold at 0.35 V for 60 minutes. Prior to each limiting-current experiment, the MEAs were conditioned again with 4 cyclic-voltammetry cycles. The limiting current was obtained with potential hold at 0.35 V (see supporting information). A quasi steady state was reached within less than a minute, and the current was recorded after 2 minutes. The working electrode feed gas was then switched to pure argon and the resulting current was recorded 1 minute later. This current represents the hydrogen crossover from the counter electrode through the membrane. Typical values were ca. 35 mA/cm² for the diluted hydrogen limiting current and ~1 mA/cm² for the crossover current. The supporting information shows a sample experimental trace.

Following Hwang and Weber [24], the effective diffusivities of DM were measured as a function of water saturation. Before each experiment, DM samples were submerged in water and kept inside a desiccator for several hours to ensure full wetting. Just before assembling the cell, the DM samples were taken out of the water and excess water was thoroughly removed from the DM surface in order not to wet the flow field or CL in the course of the cell assembly. This procedure resulted in initial sample saturations of 80 to 90%, based on sample weight and dry porosity. Before and after each experiment, the saturation of the sample was measured gravimetrically. Saturation in the DM decreased by about 10% during assembly, measurement and disassembly. The average saturation from the two measurements was used in equation 8 for the analysis of the data. Starting from a highly saturated sample, the experiment was repeated until the sample was completely dry.

Materials

Membrane-electrode assemblies (MEAs) were obtained from Ion-Power Inc. The reference electrode composition was kept the same throughout all samples, with 0.4 mg/cm^2 platinum on Vulcan XC-72 carbon support. Pt/C with platinum loadings of 0.025, 0.24, and 0.4 mg/cm^2 were used, along with different ionomer to carbon ratios (I/C, “half ionomer” and “full ionomer” where the full ionomer roughly corresponds to 0.9 ionomer:carbon ratio by weight), and Pt black as the working electrode CL as denoted in Table 1. DM with and without MPLs and with varying amounts of added PTFE (SGL Sigracet 24BC, 24AA, 24BA, 24CA, and 24EA, Freudenberg H2315, and MRC 040) were used as specified in Table 2. MEAs were used as-received, as pre-boiling in DI-water and/or sulfuric acid showed no performance improvements for the hydrogen-pump setup.

Table 1: Overview of MEAs used in this study

Type	Pt loading	Thickness (µm)	Ionomer	I/C
Pt black	4 mg/cm²	~15	Nafion	-
Pt/C	0.4 mg/cm²	~20	Nafion	'100%'
Pt/C	0.4 mg/cm²	~20	Nafion	'50%'
Pt/C	0.24 mg/cm²	~20	Nafion	'100%'
Pt/C	0.025 mg/cm² - 0.031 mg/cm²	~10	Nafion	0.63
Pt/C	0.025 mg/cm² - 0.031 mg/cm²	~10	Nafion	0.9
Pt/C	0.025 mg/cm² - 0.031 mg/cm²	~10	Nafion	1.17
Pt/C	0.025 mg/cm² - 0.031 mg/cm²	~10	3M	0.63
Pt/C	0.025 mg/cm² - 0.031 mg/cm²	~10	3M	0.9
Pt/C	0.025 mg/cm² - 0.031 mg/cm²	~10	3M	1.17

Table 2: Data of DM samples used in this study.

Type	Average Thickness (mm)	wt-% PTFE	Microporous Layer
SGL 24 AA	0.195	0	no
SGL 24 BA	0.202	5	no
SGL 24 BC	0.255	5	yes
SGL 24 CA	0.206	10	no
SGL 24 DA	0.206	20	no
SGL 24 EA	0.206	30	no
MRC 040	0.190	0	no
MRC 040+PTFE	0.210	4	no
Freudenberg H2315	0.200	0	no

Results and discussion

DM effective properties and resistances

Experiments at different gas pressures with one to five DM stacked upon each other were conducted. The experimental data was analyzed according to equations 3 through 10. Equation 6 predicts that the transport resistance of the cell increases linearly with the number of DM, which was confirmed in the experiment as shown in Figure 3. In the figure, the ordinate axis intercept represents the CL resistance. The average DM resistance can be obtained via a linear fit using equation 6. The DM resistances at one, two and three bar absolute reveal that the DM resistance is proportional to pressure (~1.0 to 1.2 p). This indicates that the transport is governed by molecular diffusion (see equations 9 and 10), in agreement with other works in the field [4, 8, 9]. Using the stacking method, the transport resistance of a range of commercially available DM was quantified and is presented in the supporting info.

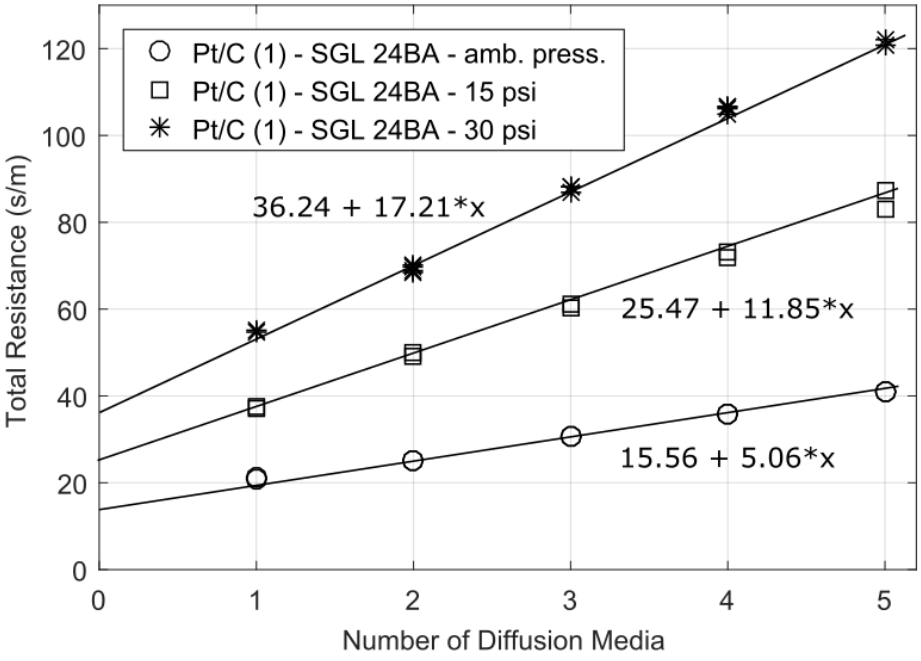

Figure 3: Diffusion resistance vs. number of DM for different operating pressures. Values were derived from a linear function. The ordinate intercept represents the corresponding CL resistance.

Different DM with varying PTFE loading from SGL were investigated. While PTFE helps water management with multiphase liquid and vapor flow under wet conditions, under dry conditions, however, the transport resistance through the DM is expected to increase with the addition of PTFE [22, 33]. This effect is seen in Table 3, where the effective diffusivity ratio steadily decreases from 0.43 to 0.16 as more PTFE is added to the SGL 24 series substrate. Following LaManna et al. [34], the effect on tortuosity of PTFE loading was calculated as

$$\frac{D_{eff}}{D} = f(\varepsilon) = \varepsilon/\tau \qquad [11]$$

The tortuosity in the SGL 24 series was found to increase with increasing PTFE loading, especially at PTFE contents higher than 20 wt-% as shown in Table 3.

wt-% PTFE		0	5	10	20	30	40
Porosity	SGL 24 series	0.88	0.87	0.85	0.82	0.80	-
D_{eff}/D	SGL 24 series	0.43	0.4	0.34	0.26	0.16	-
Tortuosity	SGL 24 series	2.05	2.18	2.50	3.15	5.00	-
Tortuosity	Toray-H-120 [LaManna]	2.23	-	2.83	2.87	-	6.16

Table 3: Tortuosity change with PTFE loading

The effective diffusivity as a function of saturation was investigated using DM substrates of the type MRC 105, MRC 040 and SGL Sigracet AA. As shown in figure 4a, the effective

diffusivity varies between DM types, which is probably largely due to differences in the structures' porosities. However, if the measured effective diffusivities are normalized by those of the dry DM [24] according to

$$g(S) = \frac{<D>}{D}\frac{1}{f(\varepsilon)} \quad [12]$$

all DM follow a similar trend.

The restriction of gas diffusion by liquid saturation in porous media is typically modeled as an exponential function of the saturation S [24, 35, 36]:

$$g(S) = (1 - S)^n \quad [13]$$

An exponent of $n = 5$ in equation 13 was found to fit the data well. This is higher than that seen with other GDLs in the literature (n ~ 3.2) using similar techniques [23, 24], which may be due to the structure of the MRC GDLs [22] although SGL shows a similar trend. Although this value is higher than other studies, it does agree with Shiomi et al. [37] who found $5 < n < 6$ using neutron imaging, and the pore-network modeling of Gostick et al. [36] who estimated an upper limit of $n = 5$. To analyze the sensitivity towards the loss of saturation during the experiment, the data was fitted assuming the actual saturation to be 10% higher/lower than the measured saturation, which resulted in $4.5 < n < 5.5$.

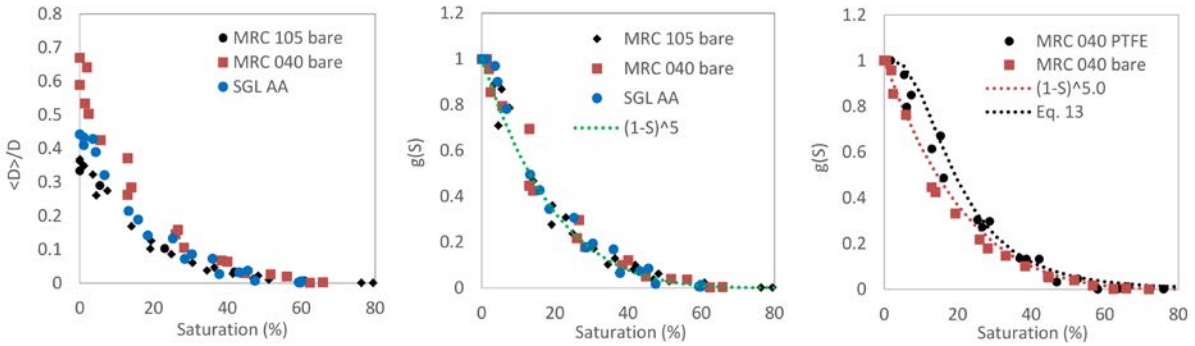

Figure 4: (a) measured effective diffusivity, <D>/D and (b) normalized saturation function, g(S), with respect to saturation. (c) Normalized saturation function with respect to saturation for MRC with and without PTFE; also shown is equation 14 fit.

To investigate if the addition of PTFE changes the effect of saturation on $g(S)$, MRC 040 without and with added PTFE (ca. 5 wt-%) were compared as shown in Figure 4c (see supporting information for effective diffusivity). The differences in partially saturated conditions are relatively small, however the shape of the normalized saturation function of the MRC 040 DM changes with PTFE and does not follow the relationship in equation 13. This is in agreement with Hwang and Weber [24] who examined other GDLs. In their study, an empirical relation was proposed of the form

$$g(S) = \frac{1}{2}\left\{1 + erf\left[-\frac{\ln(S)+a}{b}\right]\right\} \qquad [14]$$

where *a* and *b* are fit parameters. For MRC 040, the fit shown in figure 4c was obtained with $a = 1.65$ and $b = 0.88$. It should be noted that the values given here are for the entire GDL, which results from a non-uniform saturation through the thickness [38], and thus these relationships do not necessarily apply locally as recently discussed [39].

What is surprising is the magnitude of the intercept in Figure 3, which suggests a non-negligible CL resistance even with fast hydrogen kinetics. In fact, the relative contributions of

DM and CL to the overall transport resistance are shown in Figure 5. The figure demonstrates that most of the resistance for a dry electrode is in the CL, with about equal portions in the GDL and MPL. The magnitude of the MPL to GDL resistance is in agreement with Chan et al [3], who found that the presence of an MPL reduces the effective diffusivity of a DM by around 42%. Viscous permeability measurements by Carrigy et al. [21] also show a similar trend. Both suggest the major transport process in MPLs is Knudsen diffusion due to much smaller pore sizes in comparison to the carbon-fiber substrate.

Figure 5: Breakdown of total transport resistance into contribution of CL, GDL, and MPL. The contribution of the MPL is derived from a comparison of SGL 24 BA (no MPL) and SGL 24 BC (w/ MPL).

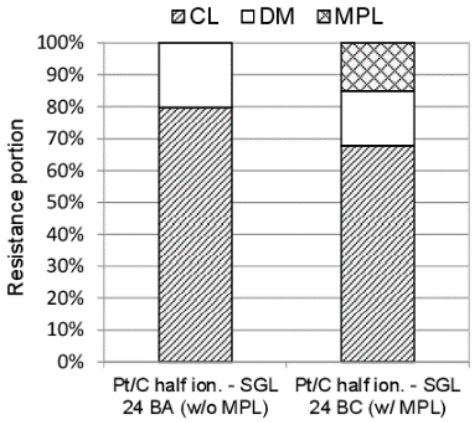

To assess the pressure-independent transport contribution in a DM, the stacking experiment was performed using one to five SGL 24BC diffusion media at 1, 2, and 3 atm pressures. The resistance follows ~0.56*p (see supporting information), indicating ~56% molecular diffusion and ~44% Knudsen diffusion in the MPL-coated GDL. Assuming that the resistance contributions of GDL and MPL estimated in Figure 5 are correct and that transport inside the GDL is dominated by molecular diffusion, as Figure 3 suggests and was observed throughout this study, 94% of the MPL resistance can be related to Knudsen diffusion.

Catalyst-Layer resistances

The stacking experiment shown in Figure 3 serves to determine CL transport resistance as well. CLs investigated were platinum black and Pt/C featuring platinum loadings ranging from 0.4 mg/cm² to 0.025 mg/cm² and two I/C ratios. Averaged transport resistances found in these CLs are presented in Figure 6. As expected, transport resistance of Pt/C CLs increased with decreasing platinum loading [4, 6, 7, 26, 30]. While resistance increased by about 15% going from a platinum loading of 0.4 mg/cm² to 0.24 mg/cm², it increased disproportionally by 126% going from 0.24 mg/cm² to 0.028 mg/cm². This is in qualitative agreement with other studies [2, 7, 26]. Reduced ionomer content, probably resulting in a thinner film covering the reaction sites (figure 1) and lower bulk diffusion resistance [40], resulted in a substantially lower transport resistance.

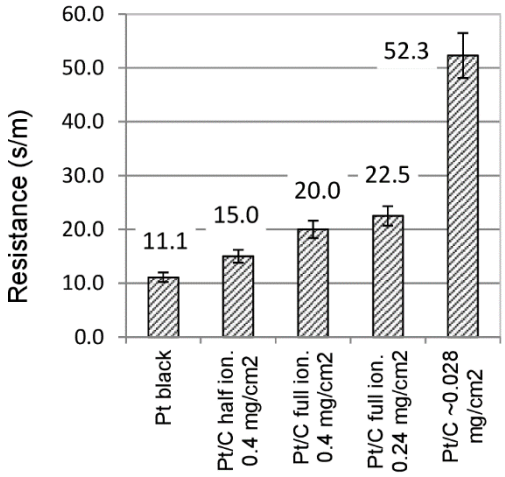

Figure 6: Transport resistances of a Pt black CL and Pt/C CL featuring different Pt loadings. Transport resistances increase disproportionally with decreasing Pt loadings. The error bars represent the root-mean-square deviations.

Varying the pressure reveals that the transport resistance in CL is significantly less dependent on pressure than in the DM, following ~0.66*p. Taking into account the small pore sizes of the CL, Knudsen diffusion is expected to dominate the transport in the bulk of the CL [1, 4, 8], which is not pressure-dependent according to equation 10. The apparent 0.66*p-dependence may be rationalized by some molecular diffusion in the bulk and transport into the ionomer film (figure 1) in the form of a pressure-dependent sorption or transport process locally, as well as perhaps deviation from the assumption of a linear gradient in concentration that was used to analyze the data; the exact cause is still under examination.

The idea of a local resistance at the platinum sites is linked to the interface of the platinum particles, ideally covered by an ionomer film. The findings in Figure 6 suggests that this could be the cause. To investigate this concept, two different ionomers, Nafion

(1100 EW, Equivalent Weight) and 3M ionomer (825 EW), were used in low-platinum loaded Pt/C CLs at two different I/C ratios: 0.63 and 1.17. Overall, resistances of Pt/C with Nafion and 3M were in the same range, although 3M has higher sulfonic-acid groups and water content at least in a thin film [41], which is related to the expected water content in the CL [42]. Since the transport properties of the membranes are a function of water content, they should be more resistive in the CL, in agreement with the data, and 3M ionomer should demonstrate slightly improved results (i.e., lower resistance) as shown in Figure 7. This improvement at low I/C ratio seemingly vanishes at the higher I/C ratio due to the increased amount of the thickness of the ionomer films and mainly its impact in decreasing the overall porosity of the CLs and increases gas-transport resistance [43, 44]. This is also in agreement with the lower resistance using the half-ionomer amount in Figure 6, although at the higher loadings the different in total resistance value is less significant. Of course, a minimal I/C ratio is required for percolation and proton conduction through the layer, which is perhaps why the CL resistance with Nafion is higher in the 0.63 I/C ratio than in the data in Figure 6 that was obtained with an I/C ratio of closer to 0.9 for the full-ionomer CL; however, there was significant scatter in the data.

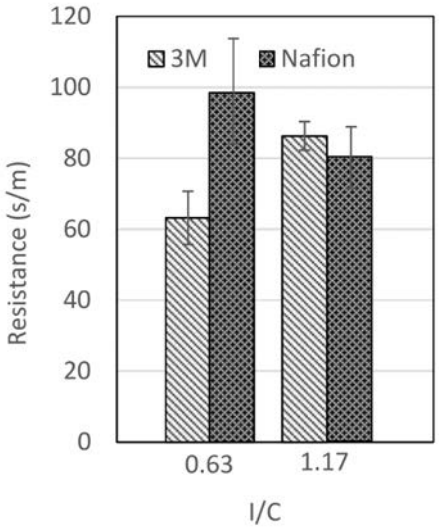

Figure 7: Measured resistance of 0.025 mg/cm^2 Pt/C CLs prepared with 3M and Nafion ionomer at I/C ratios of 0.63 and 1.17. 3M ionomer (lower EW), has an advantage over Nafion at low I/C, which vanishes at high I/C. The error bars represent the root-mean-square deviations.

Resistances mass dependence

Switching the reacting gas from hydrogen to deuterium was used to determine to which extent the transport resistances were dependent on molecular mass. As discussed earlier, molecular and Knudsen diffusion should decrease by a factor of around $\sqrt{2}$ when replacing hydrogen by deuterium. This approach was combined with stacking of DM to get experimental access to individual resistances of CLs and DM as well. Figure 8 shows that the ratio of hydrogen and deuterium resistances of a SGL 24BA decreases by $\sqrt{2}$, in agreement with the expected diffusion-dominated response. Interestingly, the ratio of hydrogen and deuterium resistances is smaller than $\sqrt{2}$ in CLs. Hence, the overall transport resistance has a weaker dependence on molecular mass than diffusion, thereby indicating that non-diffusional transport, which may have no molecular weight-dependence, but which may be proportional to flux density as discussed above, plays a role in CLs. Except for kinetics

depending on mass, deuterium and hydrogen have identical chemical properties. It seems likely that a chemical process like adsorption/desorption, potentially at the surface of the ionomer film covering platinum particles, is responsible for a portion of the overall transport resistance. This mass-independent portion increases with decreasing loading, suggesting a non-diffusional resistance that scales with platinum loading, corresponding to an interfacial resistance. If one assumes the coexistence of diffusion and a second transport mechanism that is completely molecular mass-independent, this second transport mode would be responsible for ca. 15% of the overall resistance in the case of the 0.4 mg/cm² Pt/C CLs and ca. 45% in the case of the 'low-Pt' Pt/C CLs.

Figure 8: Ratio of deuterium and hydrogen transport resistances of different Pt/C catalyst layers and of a GDL. Dashed and solid line represent the expected ratio for a purely molecular or Knudsen diffusional transport, respectively.

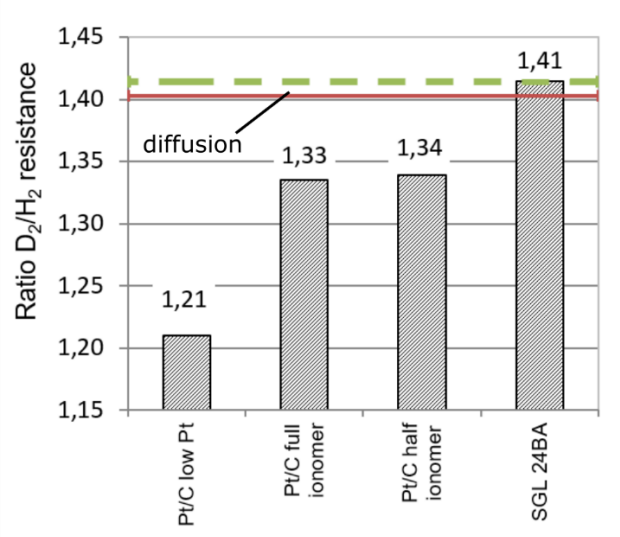

Summary

The hydrogen limiting-current method was used for the quantification of various fuel-cell transport limitations. It was shown that the transport resistances of DM and CL can be separated by linear interpolation of experiments using different numbers of DM. The transport properties of various commercial DM such as SGL Sigracet 24 series and MRC 040 with and without added PTFE under dry and partially saturated conditions were discussed. It was shown that under dry conditions, addition of PTFE decreases the effective diffusivity of DM due to decreasing porosity and increasing tortuosity. In partially saturated conditions, however, addition of PTFE increases the normalized effective diffusivity $g(S)$ at low to medium saturation levels which, for MRC follows a relationship of $g(S) = (1 - S)^5$.

Surprisingly, the hydrogen-limiting current with dry DM is dominated by the CL resistance. This resistance was explored for different CLs, including loadings and ionomer type and amount. The CL resistance in this experiments mirrored other findings based on oxygen limiting current studies that decreased Pt loadings results in much higher transport resistance. In addition, changing from hydrogen to deuterium demonstrated that there is a non-diffusional resistance contribution being responsible for 15% to 45% of the total transport resistance, which increased as platinum loading decreased. This transport resistance may be related to an adsorption/desorption process at the interface of the ionomer covering the platinum sites. In terms of ionomer, lower I/C yielded lower resistances, with a benefit of 3M short-side chain, lower equivalent-weight ionomer, which may be due to its enhanced oxygen transport and thin-film morphology compared to Nafion. Work on elucidating the additional resistances in CL at low platinum loadings using the hydrogen limiting-current method is ongoing including temperature and humidity studies.

Overall, the alternative use of hydrogen and deuterium, along with a variation of the pressure of the feed gases and a variation of cell temperature (not included in this study), while operating under controlled humidity, make the limiting current method a powerful tool for investigating fuel cell transport properties. In comparison to the oxygen limiting current method, problems due to water generation can be avoided. In comparison to ex-situ methods using cast ionomer films on platinum electrodes, however, the experimentalist can be confident to operate a measurement that represents the original microstructure and transport pathways of CL. The technique is a viable means of investigating gas-transport resistances of various fuel-cell components without complications induced by other methods, and provides an interesting perspective and additional knowledge into the limiting mechanisms.

Acknowledgements

The Authors would like to thank Anna Freiberg and Gisuk Hwang for discussions as well as Nobuaki Nonoyama for very helpful insights. The work was funded under the Fuel Cell Performance and Durability Consortium (FC-PAD), by the Fuel Cell Technologies Office (FCTO), Office of Energy Efficiency and Renewable Energy (EERE), of the U.S. Department of Energy under contract number DE-AC02-05CH11231 and Program Development Managers Dimitrios Papageorgopoulos and Greg Kleen.

References

1. Weber, A.Z., et al., *A Critical Review of Modeling Transport Phenomena in Polymer-Electrolyte Fuel Cells.* Journal of the Electrochemical Society, 2014. **161**(12): p. F1254-F1299.
2. Weber, A.Z. and A. Kusoglu, *Unexplained transport resistances for low-loaded fuel-cell catalyst layers.* J. Mater. Chem. A, 2014. **2**(41): p. 17207–17211.
3. Kongkanand, A. and M.F. Mathias, *The Priority and Challenge of High-Power Performance of Low-Platinum Proton-Exchange Membrane Fuel Cells.* journal of Physical Chemistry Letters, 2016. **7**(7): p. 1127-1137.
4. Nonoyama, N., et al., *Analysis of Oxygen-Transport Diffusion Resistance in Proton-Exchange-Membrane Fuel Cells.* Journal of The Electrochemical Society, 2011. **158**(4): p. B416.
5. Sakai, K., et al., *Analysis of Reactant Gas Transport in Catalyst Layers - Effect of Pt-loadings.* 2009. **25**(1): p. 1193–1201.
6. Greszler, T.a., D. Caulk, and P. Sinha, *The Impact of Platinum Loading on Oxygen Transport Resistance.* Journal of The Electrochemical Society, 2012. **159**(12): p. F831-F840.
7. Ono, Y., et al., *The Analysis of Performance Loss with Low Platinum Loaded Cathode Catalyst Layers*, in *ECS Transactions*. 2010. p. 69–78.
8. Beuscher, U., *Experimental Method to Determine the Mass Transport Resistance of a Polymer Electrolyte Fuel Cell.* Journal of The Electrochemical Society, 2006. **153**(9): p. A1788.
9. Baker, D.R., et al., *Measurement of Oxygen Transport Resistance in PEM Fuel Cells by Limiting Current Methods.* Journal of The Electrochemical Society, 2009. **156**(9): p. B991.
10. Baker, D.R., et al., *The Use of Limiting Current to Determine Transport Resistance in PEM Fuel Cells*, in *ECS Transactions*. 2006, Ecs. p. 989–999.
11. Caulk, D.a. and D.R. Baker, *Heat and Water Transport in Hydrophobic Diffusion Media of PEM Fuel Cells.* Journal of The Electrochemical Society, 2010. **157**(8): p. B1237.
12. Zamel, N., et al., *Experimental measurements of effective diffusion coefficient of oxygen–nitrogen mixture in PEM fuel cell diffusion media.* Chemical Engineering Science, 2010. **65**(2): p. 931–937.
13. Chan, C., et al., *Experimental measurement of effective diffusion coefficient of gas diffusion layer/microporous layer in PEM fuel cells.* Electrochimica Acta, 2012. **65**: p. 13–21.
14. Unsworth, G., L. Dong, and X. Li, *Improved experimental method for measuring gas diffusivity through thin porous media.* AIChE Journal, 2013. **59**(4): p. 1409–1419.
15. Carrigy, N.B., et al., *Knudsen Diffusivity and Permeability of PEMFC Microporous Coated Gas Diffusion Layers for Different Polytetrafluoroethylene Loadings.* Journal of The Electrochemical Society, 2012. **160**(2): p. F81-F89.
16. Mangal, P., et al., *Experimental study of mass transport in PEMFCs: Through plane permeability and molecular diffusivity in GDLs.* Electrochimica Acta, 2015. **167**: p. 160-171.
17. Ismail, M.S., et al., *On the through-plane permeability of microporous layer-coated gas diffusion layers used in proton exchange membrane fuel cells.* International Journal of Hydrogen Energy, 2011. **36**(16): p. 10392-10402.
18. Ismail, M.S., et al., *Effect of polytetrafluoroethylene-treatment and microporous layer-coating on the in-plane permeability of gas diffusion layers used in proton exchange membrane fuel cells.* Journal of Power Sources, 2010. **195**(19): p. 6619-6628.

19. Orogbemi, O.M., et al., *The effects of the composition of microporous layers on the permeability of gas diffusion layers used in polymer electrolyte fuel cells.* International Journal of Hydrogen Energy, 2016. **41**(46): p. 21345-21351.

20. Kramer, D., et al., *Electrochemical diffusimetry of fuel cell gas diffusion layers.* Journal of Electroanalytical Chemistry, 2008. **612**(1): p. 63–77.

21. Flückiger, R., et al., *Anisotropic, effective diffusivity of porous gas diffusion layer materials for PEFC.* Electrochimica Acta, 2008. **54**(2): p. 551–559.

22. Zenyuk, I.V., et al., *Gas-diffusion-layer structural properties under compression via X-ray tomography.* Journal of Power Sources, 2016. **328**: p. 364–376.

23. Rosen, T., et al., *Saturation Dependent Effective Transport Properties of PEFC Gas Diffusion Layers.* Journal of The Electrochemical Society, 2012. **159**(9): p. F536-F544.

24. Hwang, G.S. and a.Z. Weber, *Effective-Diffusivity Measurement of Partially-Saturated Fuel-Cell Gas-Diffusion Layers.* Journal of The Electrochemical Society, 2012. **159**(11): p. F683-F692.

25. Mashio, T., et al., *Analysis of Reactant Gas Transport in a Catalyst Layer*, in *ECS Transactions*. 2007, Ecs. p. 529–540.

26. Owejan, J.P., J.E. Owejan, and W. Gu, *Impact of Platinum Loading and Catalyst Layer Structure on PEMFC Performance.* Journal of The Electrochemical Society, 2013. **160**(8): p. F824-F833.

27. Iden, H., et al., *Relationship between gas transport resistance in the catalyst layer and effective surface area of the catalyst.* Journal of Electroanalytical Chemistry, 2013. **694**: p. 37–44.

28. Shi, S., et al., *Impact of hygrothermal aging on structure/function relationship of perfluorosulfonic-acid membrane.* Journal of Polymer Science Part B: Polymer Physics, 2016. **54**(5): p. 570-581.

29. Kudo, K., R. Jinnouchi, and Y. Morimoto, *Humidity and Temperature Dependences of Oxygen Transport Resistance of Nafion Thin Film on Platinum Electrode.* Electrochimica Acta, 2016. **209**: p. 682-690.

30. Yoon, W. and A.Z. Weber, *Modeling Low-Platinum-Loading Effects in Fuel-Cell Catalyst Layers.* Journal of The Electrochemical Society, 2011. **158**(8): p. B1007.

31. Debe, M., *Effect of Electrode Surface Area Distribution on High Current Density Performance of PEM Fuel Cells.* Journal of the Electrochemical Society, 2012. **159**(1): p. B53-B66.

32. Gostick, J.T., et al., *In-plane and through-plane gas permeability of carbon fiber electrode backing layers.* Journal of Power Sources, 2006. **162**(1): p. 228–238.

33. Fishman, Z. and A. Bazylak, *Heterogeneous Through-Plane Porosity Distributions for Treated PEMFC GDLs I. PTFE Effect.* Journal of The Electrochemical Society, 2011. **158**(8): p. B841.

34. LaManna, J.M. and S.G. Kandlikar, *Determination of effective water vapor diffusion coefficient in pemfc gas diffusion layers.* International Journal of Hydrogen Energy, 2011. **36**(8): p. 5021-5029.

35. Nam, J.H. and M. Kaviany, *Effective diffusivity and water-saturation distribution in single- and two-layer PEMFC diffusion medium.* International Journal of Heat and Mass Transfer, 2003. **46**(24): p. 4595-4611.

36. Gostick, J.T., et al., *Pore network modeling of fibrous gas diffusion layers for polymer electrolyte membrane fuel cells.* Journal of Power Sources, 2007. **173**(1): p. 277-290.

37. Shiomi, T., et al., *Effect of Liquid Water Saturation on Oxygen Transport in Gas Diffusion Layers of Polymer Electrolye Fuel Cells.* Proceedings of the Asme 8th International Conference on Fuel Cell Science, Engineering, and Technology 2010, Vol 1, 2010: p. 667-676.

38. Zenyuk, I.V., et al., *Probing water distribution in compressed fuel-cell gas-diffusion layers using X-ray computed tomography.* Electrochemistry Communications, 2015. **53**: p. 24-28.

39. García-Salaberri, P.A., et al., *Effective diffusivity in partially-saturated carbon-fiber gas diffusion layers: Effect of through-plane saturation distribution.* International Journal of Heat and Mass Transfer, 2015. **86**: p. 319-333.

40. Suzuki, A., et al., *Ionomer content in the catalyst layer of polymer electrolyte membrane fuel cell (PEMFC): Effects on diffusion and performance.* International Journal of Hydrogen Energy, 2011. **36**(3): p. 2221-2229.

41. Kusoglu, A., T.J. Dursch, and A.Z. Weber, *Nanostructure/Swelling Relationships of Bulk and Thin-Film PFSA Ionomers,.* Advanced Functional Materials, 2016. **26**(4961-4975).

42. Kusoglu, A., et al., *Water Uptake of Fuel-Cell Catalyst Layers.* Journal of the Electrochemical Society, 2012. **159**(9): p. F530-F535

43. Iden, H., et al., *Analysis of Proton Transport in Pseudo Catalyst Layers Influence of Ionomer Content.pdf>.* ECS Transactions, 2009. **25**: p. 907-921.

44. Modestov, A.D., et al., *Cathode catalyst layers with ionomer to carbon mass ratios in the range 0–2 studied by electrochemical impedance spectroscopy, cyclic voltammetry, and performance measurements.* Journal of Power Sources, 2014. **272**: p. 735-742.